

# Real Time Compensation Algorithm for Air-Gapped Current Transformers Saturation Effects

F. A. Pereira, F. C. F. Guerra, B. A. Sousa, E. N. A. Santos, N. S. D. Brito, U. A. Carmo

**Abstract**—A platform implemented with Digital Signal Controllers (DSCs) developed for real time studies of the dynamic behavior of the air-gapped current transformers (CTs) used in power grid protection and measurement systems is presented. The implemented algorithms simulate the fault current in an electric power system as well as the transient response of the current transformer. It is also presented a method of correcting the distortion of the current transformer secondary current which has a negligible value of remanent flux. For this, a tertiary winding must be available and accessible. Thus, the ratio and phase errors, as well as the distortions produced in secondary current due the core saturation in fault situations are properly corrected. Several cases were tested and the results indicate that the proposed method proved to be very effective in improving the performance of protection schemes based on the current measurement.

**Keywords:** distortion, power system protection, saturation, air-gapped CTs, real time simulation, waveform compensation.

## I. INTRODUCTION

THE fault currents in electric power systems present a sinusoidal component plus a dc decaying component. The first produces a sinusoidal magnetic flux in the current transformer (CT) core. The second produces an initially increasing flux which may lead to a high saturation level in the core. This may cause severe distortions in the secondary current supplied to protective relays. As consequences, the following problems may arise [1]:

1. Relays can operate inadequately.
2. Relays may not be sensitive to the distortions that reduce the root-mean-square value of the secondary current.
3. Relay operation may be delayed, for the reason cited in the previous item.
4. Fault locators may not show the correct indication.

Those occurrences can cause thermal and electrodynamic damages, loss of coordination in the protection relays, and difficulty of location of the faulted point, or loss of system stability. Then, it is necessary to develop techniques that provide the best accuracy in the process of transformation, to

avoid such disturbances. This task has been accomplished by several methods and mathematical tools used in the area of digital signal processing, applicable to the field of power system protection.

The initial works about the mitigation of the distortions in secondary currents of CTs considered the problem by means of hardware [2]-[3]. With the development of microprocessors, numerical techniques for detection of the CT core saturation and correction of the secondary current waveform were developed. Conrad and Oeding [4] is the first reference about this matter. The authors proposed a method in which the magnetic flux is obtained by numerical integration of the secondary current. In addition, a function that describes the minor hysteresis loops in the iron core is used to obtain the excitation current. So, the correction is performed adding this current to the distorted secondary current. A similar method was proposed by [5]. Additionally, a method to calculate the core flux prior to the fault was presented, which was based on the periodicity of the flux waveform in the steady state. The algorithm was tested in real time using a Digital Signal Processor (DSP). The reported results were good. However, this technique was not able to estimate the residual flux in the CT core. The same authors presented a method to detect the instants of the core saturation, which was based on third order difference functions [6]. Later, this method was combined with another based on second order difference functions to estimate the initial flux in the CT core [7].

The discrete wavelet transform was proposed by [8] to detect the CT saturation, in conjunction with a regression technique destined to correct the secondary current wave. Methodologies based on least squares curve fitting were presented by [9]-[11]. Despite the refined mathematical treatment, these methods impose an intense burden of computation to the relay. A simple method to reconstruct the primary current waveform is suggested in [12]. However, the accuracy might degrade if the primary fault current contains harmonics and noise.

Techniques based on artificial neural networks (ANNs) for detection and correction were proposed by [13]-[15]. These methods might require a substantial amount of network training.

The technique adopted in this work is the numerical correction of the distorted secondary current based on the estimation of the excitation current value, which, when added to the distorted secondary current, gives the value of the reflected primary current in the secondary winding. In conventional methods, using iron-cored CTs, the distorted

---

This work was supported in part by Companhia Hidroelétrica de São Francisco (Chesf), Brazil. The authors are with Federal University of Campina Grande (UFCG) – Brazil, Post-Graduate Program in Electrical Engineering - PPGEE – COPELE.

(e-mails: fagner.pereira@ee.ufcg.edu.br, chagas@dee.ufcg.edu.br, benemar@dee.ufcg.edu.br, ericson.santos@ee.ufcg.edu.br, nubia@dee.ufcg.edu.br, uacarmo@chesf.gov.br).

Paper submitted to the International Conference on Power Systems Transients (IPST2015) in Cavtat, Croatia June 15-18, 2015

secondary current is integrated to obtain the flux linkage imposed by the primary current. This flux is added to the remaining amount of flux and then, by using a model characterizing the magnetic core of the CT, the excitation current is estimated. So, the knowledge of the remaining flux value in the core, CT load characteristics and secondary winding impedance, which in practice are not easy to be obtained with accuracy, are needed in this approach. In the proposed method, the flux linkage is obtained by integrating the voltage on a tertiary winding, which must be available and accessible, which can also be easily found in commercially current transformers. Thus, knowledge of the secondary winding impedance is not necessary. Further, with an open core, the value of the remaining flux can be ignored. Thus, the excitation current is determined directly by using the saturation curve of the core and added to the distorted secondary current to obtain a faithful reproduction of the waveform of the primary current.

The following mathematical modeling of air-gapped CTs followed by the proposed method is presented. The hardware platform for real time simulation of an electrical system used as a model to validate the proposed correcting algorithm is shown. The development of a hardware and software set for acquisition and processing of the distorted secondary current signal is also described. Finally, analysis of the results from the real time implementation of the proposed method of correcting distorted waveform current in the secondary low remanence CTs winding and applicability of the method are performed.

## II. CURRENT TRANSFORMER MODEL

A way to improve the transient performance of CT is to insert air gaps in the magnetic core to reduce the remanent flux, as shown in the characteristics  $B - H$  (induction versus magnetic field) of Fig. 1

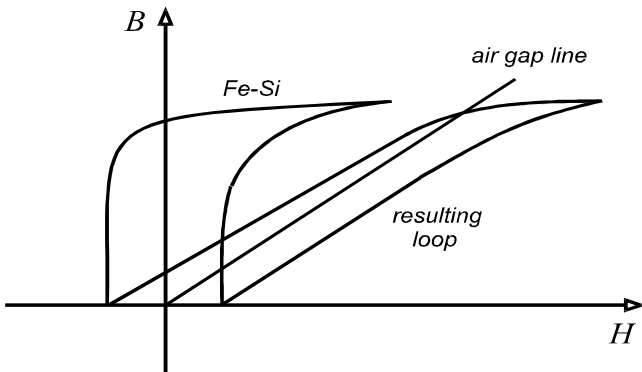


Fig. 1. Air gap effect in magnetic core of iron -silicon alloy ( Fe-Si).

The main advantages of inserting air gaps in magnetic cores are [16]: reduction of the CT secondary time constant, which implies a reduction of the core cross section area (smaller physical size) to the same operating conditions compared to the TCs with closed core; less influence of load power factor in CT response in transient regime, compared to a closed core

CT and a lower voltage appearing at the secondary terminals when they are open.

The CT equivalent electric circuit is shown in Fig. 2. A third winding (tertiary), made by a thin wire, superimposed to the secondary, is used to provide the voltage  $u_3$  that will be integrated for determination of the magnetic flux in the CT core.

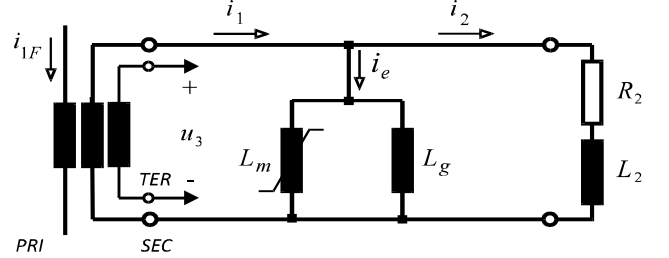


Fig. 2. The current transformer equivalent circuit.

Fig. 2 shows the total resistance and inductance of the wires and burden ( $R_2$ ,  $L_2$ ), as well as the nonlinear magnetizing inductance of the iron core ( $L_m$ ) and the linear inductance of the gap ( $L_g$ ). In this figure,  $i_{1F}$  is the primary fault current,  $i_1$  is the primary current reflected to the secondary,  $i_e$  is the excitation current,  $i_2$  is the secondary current and  $u_3$  is the induced voltage on tertiary winding.

The magnetic core properties are represented by the following expression, where  $\lambda$  is the flux linkage in the secondary winding and  $\sigma$  is the electric conductance related to the iron core losses:

$$i_e(t) = f[\lambda(t)] + \sigma \frac{d\lambda(t)}{dt}. \quad (1)$$

The function  $f[\lambda(t)]$  describes the CT saturation curve (in peak values). So, the trajectories in the phase plane  $\lambda - i_e$  describe asymmetric minor loops. The parameter  $\sigma$  is determined by trial-and-error method, by comparing dynamic loops  $\lambda - i_e$  in 60 Hz obtained by computer simulations with those registered in the laboratory.

For the circuit of Fig. 2, it follows that:

$$\lambda(t) = \lambda(t_0) + \int_0^t u_3(t) dt. \quad (2)$$

$$i_e(t) = f[\lambda(t)] + \sigma u_3(t). \quad (3)$$

$$i_1(t) = i_e(t) + i_2(t). \quad (4)$$

The term  $\lambda(t_0)$  of (2) is the remanent flux in the magnetic core,  $\lambda_R$ , plus the initial secondary flux linkage  $\lambda_0$  imposed by the primary current. The remanent flux in the magnetic core is reduced to a negligible value by the air gap (CT class TPZ). However,  $\lambda_0$  cannot be neglected because small increases of  $\lambda$  cause large increases in  $i_e$  when the core saturates.

## III. THE PROPOSED METHOD

The correction of the secondary current waveform is accomplished in accordance to the test setup block diagram shown in Fig. 3. The signal conditioning module has two inputs and two outputs connected to corresponding ports of the correction system.

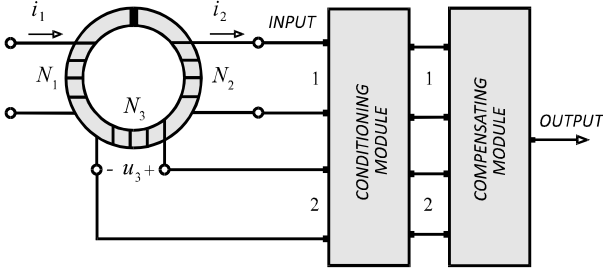


Fig. 3. Test setup block diagram of the proposed method.

The current in the secondary winding with  $N_2$  turns is applied to the input 1 of the module and converted into a proportional voltage. The third winding of the CT (tertiary), with  $N_3$  turns, is connected directly to the input 2 and the conditioned voltage  $u_3$  is numerically integrated by the correction system to provide the values of  $\lambda$ . Since there is no current flowing in the tertiary, the integration of  $u_3$  provides a suitable measure of the magnetic flux in the CT core. The third winding is necessary because the integration of the voltage in secondary winding requires an accurate knowledge of the resistance and reactance of the connecting cables to calculate the voltage drop caused by  $i_2$ . Another additional advantage of the proposed methodology is that the initial flux linkage  $\lambda(t_0)$  is measured directly by integrating the voltage  $u_3$ , and not estimated as in other techniques, like in [7].

The flowchart of the proposed correction method is illustrated in the Fig. 4 and described in the following steps.

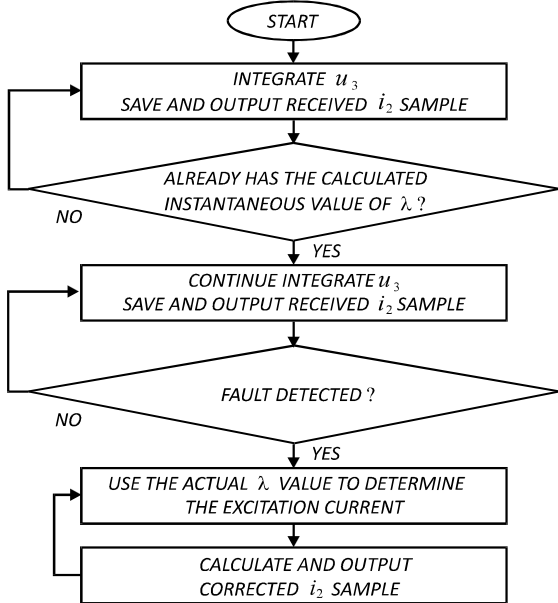


Fig. 4. General flowchart of the proposed method.

1. Initially, the system makes the numerical integration of the voltage  $u_3$ , recording after a few cycles the instantaneous value of the flux in CT core. At the same time, the value of the secondary current is sampled, recorded and sent directly to the system output.

2. The fault is detected when the secondary current exceeds a threshold value, corresponding to 150% of the nominal primary current.

3. During the fault condition, each value of  $\lambda$ , calculated by (2), is used to determine the corresponding value of the excitation current, by the use of CT saturation curve and the parameter  $\sigma$ , as established in (3).

4. For each new sample, the CT secondary current is added to the magnetization current in accordance with (4), to provide the corrected output.

The threshold value was chosen as 1.5 pu, which is usually used in overcurrent protection schemes. In this process, three consecutive samples of current are tested in order to avoid incorrect operations due to the presence of noise in the current signal.

#### IV. THE SIMULATION PLATFORM

A digital signal controller (DSC) was employed to simulate and provide three signals, in real time: the primary current, the distorted secondary current of the CT and the tertiary winding voltage to determine the flux linkage. The primary current is provided only for comparison purposes with the corrected current.

The line diagram of the simulated primary system is shown in Fig. 5. This is a typical 230 kV transmission line of the Chesf (Hydroelectric Company of São Francisco) system.

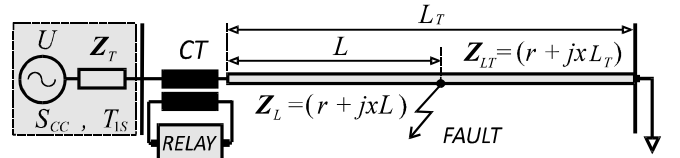


Fig. 5. Electric power system considered in the study.

In Fig. 6 is shown the single-phase equivalent circuit for simulating a fault at a distance  $L$  from the sending bus.

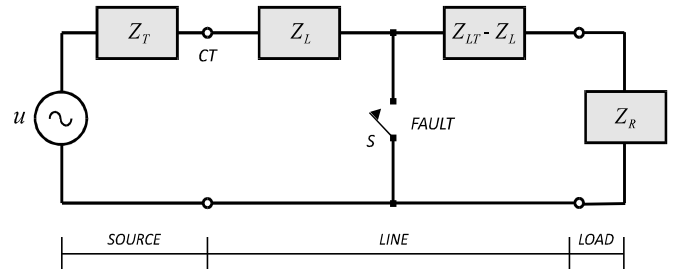


Fig. 6. Single-phase equivalent circuit of the system shown in Fig. 5.

For the circuit of Fig. 6, we can write:

$$\frac{di(t)}{dt} = \frac{u(t) - Ri(t)}{L}. \quad (5)$$

The constants  $R$  and  $L$  are, respectively, the total resistance and inductance between the voltage source and the fault;  $i$  is the current in the circuit. Thus, applying the Euler method, the primary current can be obtained by:

$$i_k = i_{k-1} + h \left. \frac{di}{dt} \right|_{k-1}, \quad (6)$$

where  $k$  is the sample order and  $h$  is the integration step used in the simulation.

For the circuit shown in Fig. 2, we can write:

$$\frac{d\lambda}{dt} = R_2 i_2(t) + L_2 \frac{di_2(t)}{dt}. \quad (7)$$

$$i_2(t) = i_1(t) - i_e(t). \quad (8)$$

$$i_e = f(\lambda). \quad (9)$$

Combining (7), (8) and (9), we have:

$$\frac{d\lambda}{dt} = \frac{R_2[i_1(t) - f(\lambda)] + L_2 \frac{di_1(t)}{dt}}{1 + L_2 \frac{df(\lambda)}{d\lambda}}. \quad (10)$$

The sample of the magnetic flux linkage is calculated by:

$$\lambda_k = \lambda_{k-1} + h \left. \frac{d\lambda}{dt} \right|_{k-1}. \quad (11)$$

The system data are the following: rated voltage,  $U_N$ : 230 kV; rated current,  $I_N$ : 800 A; line length,  $L_T$ : 85 km; series resistance,  $r$ : 0.0319  $\Omega$ /km; series reactance,  $x$ : 0.3311  $\Omega$ /km; short circuit power in 230 kV bus,  $S_{CC}$ : 7.2 GVA; time constant in 230 kV bus,  $T_{1S}$ : 35 ms; Thévenin impedance in 230 kV bus,  $Z_T = 0.56 + j 7.35 \Omega$ ; equivalent impedance in receiving bus,  $Z_R = 166 \Omega$ ; distance between fault and CT,  $L = 5$  km.

The CT has the following data: rated primary current: 900 A; rated secondary current: 5 A; core cross section:  $1.91 \times 10^{-3}$  m<sup>2</sup>; average length of magnetic path: 0.50 m; air gap length: 4 mm; stacking factor: 0.96; secondary winding resistance: 0.25 $\Omega$ ; secondary winding reactance: negligible; overcurrent factor: 20; rated secondary burden: 1  $\Omega$ .

The CT saturation curve is shown in Fig. 7.

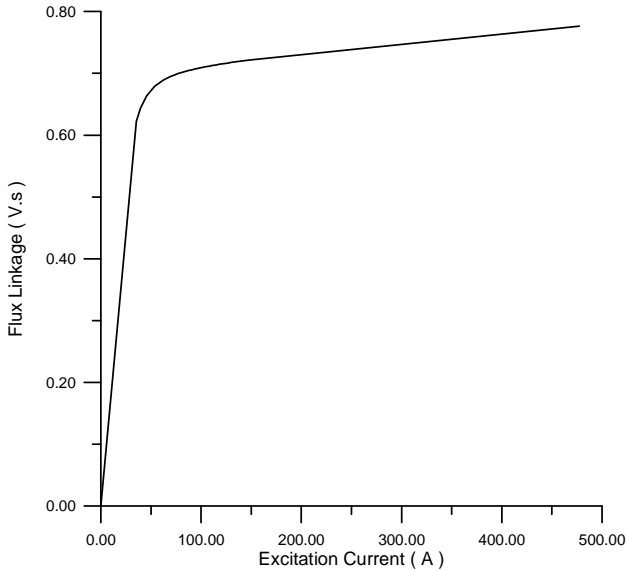


Fig. 7. Saturation curve of the air-gapped CT.

Real-time simulations were performed on a hardware platform consisting of a 32-bit digital signal controller TMS320F28335, with floating point arithmetic unit, manufactured by Texas Instruments, three 12-bit digital to analog converters DAC7621, manufactured by Burr- Brown, and three second-order low-pass filters, Butterworth type, with

cutoff frequency at 5 kHz. The block diagram of the simulation platform is shown in Fig. 8.

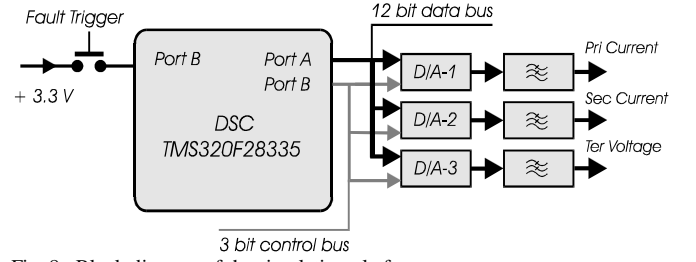


Fig. 8. Block diagram of the simulation platform.

The DSC performs real time calculations for processing the simulation algorithm. The calculations are performed at a sampling frequency of 20 kHz for future compatibility with RTDS<sup>®</sup> (Real Time Digital Simulator) systems. The calculated values are scaled and supplied in multiplexed way from the port A of DSC to a 12-bit data bus. The control bus from the port B of DSC has 3 bits, each of which is targeted to the chip selection pin of the D/A converters. When the corresponding bit is enabled, the data present on the data bus is loaded at the converter and its output is updated to the new value. The first converter (D/A-1) gives the primary current signal, the second converter (D/A-2) provides the CT secondary current signal and the third (D/A-3) provides the voltage in the tertiary winding. At every 50 microseconds, the DSC performs the following operations:

- calculates the primary current, the secondary current and the tertiary voltage;
- scales the magnitudes to 12 bits;
- writes the resulting values on the data bus, one at a time; for each written value, the control bus selects the D/A converter to update the output to the correction system.

The simulation is initiated in steady state condition. When the button “Fault Trigger” of Fig. 8 is pressed, the fault regime starts. When the button is released, the simulation goes back to the steady state condition.

The system was assembled from the development kit eZdsp<sup>™</sup> F28335, from Spectrum Digital Incorporated, connected to D/A converters, separately mounted on dedicated printed circuit boards. The programming of the DSC was done using Code Composer Studio 3.3 development environment, based on C++ programming language.

## V. THE CORRECTION PLATFORM

Figure 9 shows the block diagram of the hardware platform used to correct the distorted secondary current.

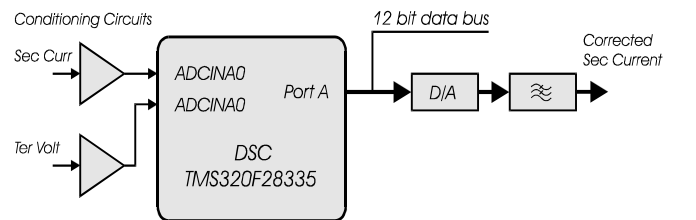


Fig. 9. Block diagram of the correction platform.

The platform consists of:

- a digital signal controller (DSC) TMS320F28335;
- two conditioning circuits for input signals;
- a 12-bits D/A converter (DAC7621);
- a low-pass filter in the output.

Two inputs of the 12-bit analog-to-digital converter (ADCINA0, ADCINA1) of the DSC are used. The first channel performs the acquisition of a voltage signal proportional to the CT secondary current. The second reads the voltage on the tertiary winding.

The acquisitions are made on a sampling frequency of 20 kHz, so the quantities are taken every 50 microseconds. After the acquisition of the signals, the main routine of the algorithm performs the correction of the secondary current.

This platform was also mounted from eZdsp™ F28335 development kit and the C++ language on the manufacturer's development environment was also used.

Figure 10 shows the two hardware platforms used in the method validation, one in the simulation of the primary system and other in the correction of the secondary current.

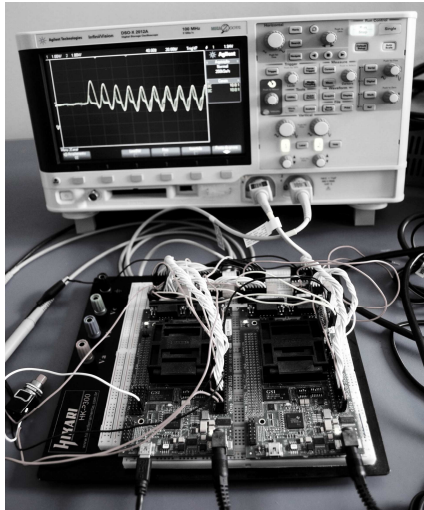


Fig. 10. Hardware implementation of the two test platforms.

## VI. RESULTS

In the simulations, three different total impedance values in the secondary winding of the CT are considered:  $1.0 + j 0.0 \Omega$ ,  $1.0 + j 1.0 \Omega$  and  $2.4 + j 0.7 \Omega$ . In all cases, the fault incidence angle is  $0^\circ$ .

To evaluate the performance of the algorithm, the transient error,  $\varepsilon_T$ , is calculated at every sampling instant [7]:

$$\varepsilon_T = \frac{k_N i_2 - i_{1F}}{\sqrt{2} I_{1F}}, \quad (12)$$

where  $k_N$  is the turns ratio of the CT,  $i_2$  is the secondary current,  $i_{1F}$  is the primary current and  $I_{1F}$  is the RMS value of this current in symmetrical regime.

Figure 11 to Fig. 13 show the primary and secondary currents. Figure 14 to Fig. 16 show the instantaneous RMS values of these currents. The transient errors are shown in Fig. 17 to Fig. 19.

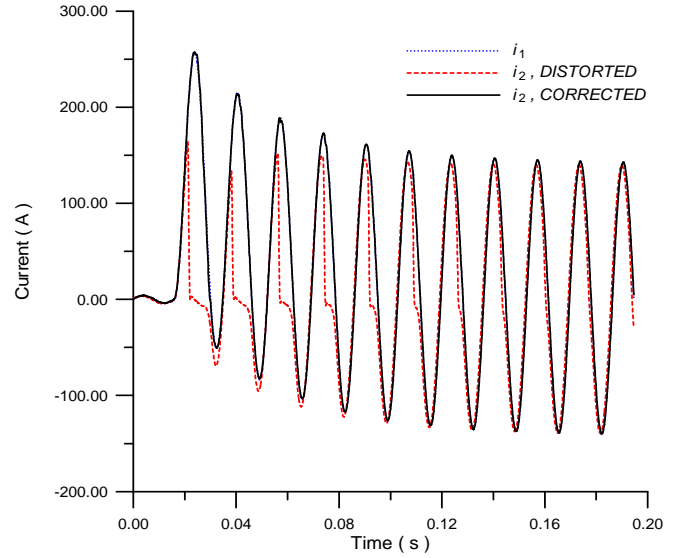


Fig. 11. Currents  $i_1, i_2$  (distorted, corrected) – Burden:  $1.0 + j 0.0 \Omega$ .

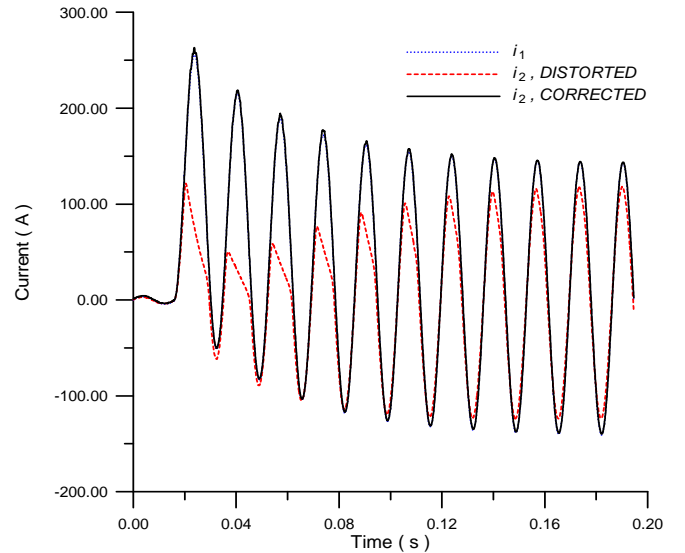


Fig. 12. Currents  $i_1, i_2$  (distorted, corrected) – Burden:  $1.0 + j 1.0 \Omega$ .

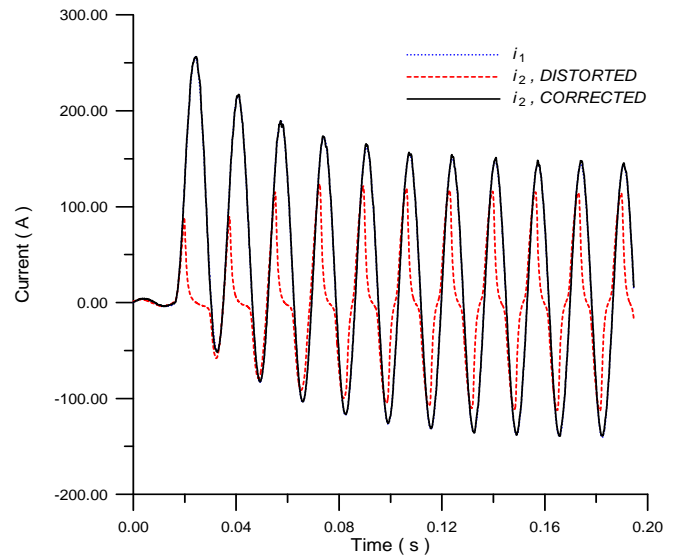


Fig. 13. Currents  $i_1, i_2$  (distorted, corrected) – Burden:  $2.4 + j 0.7 \Omega$ .

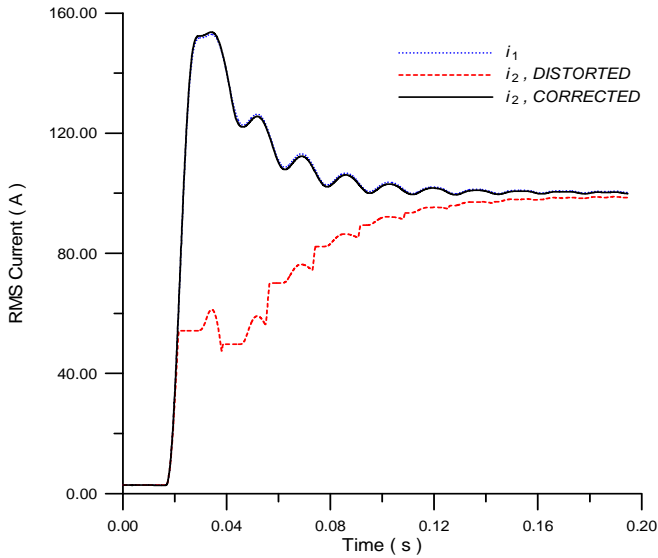


Fig. 14. RMS currents  $i_1$ ,  $i_2$  (distorted, corrected) – Burden:  $1.0 + j 0.0 \Omega$ .

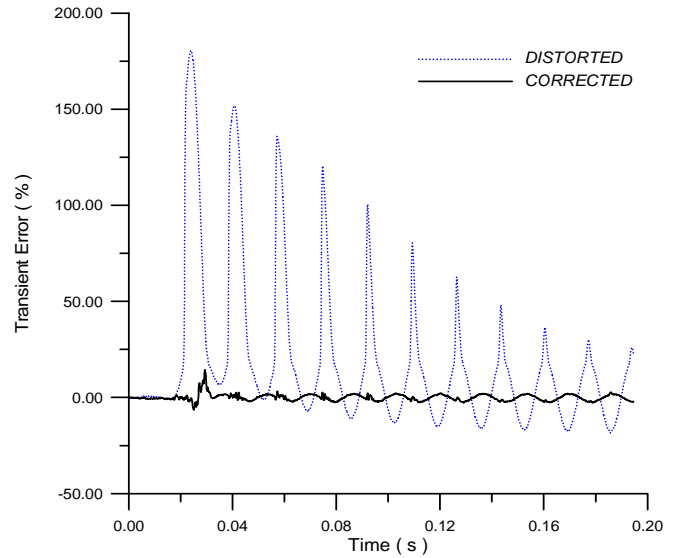


Fig. 17. Transient errors – Burden:  $1.0 + j 0.0 \Omega$ .

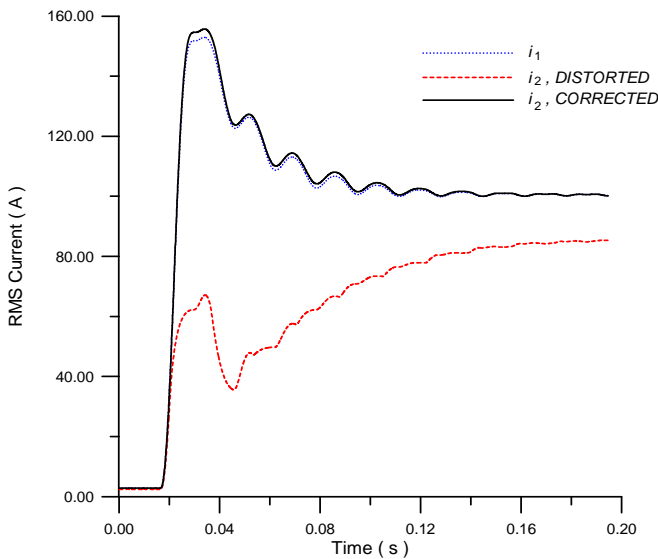


Fig. 15. RMS currents  $i_1$ ,  $i_2$  (distorted, corrected) – Burden:  $1.0 + j 1.0 \Omega$ .

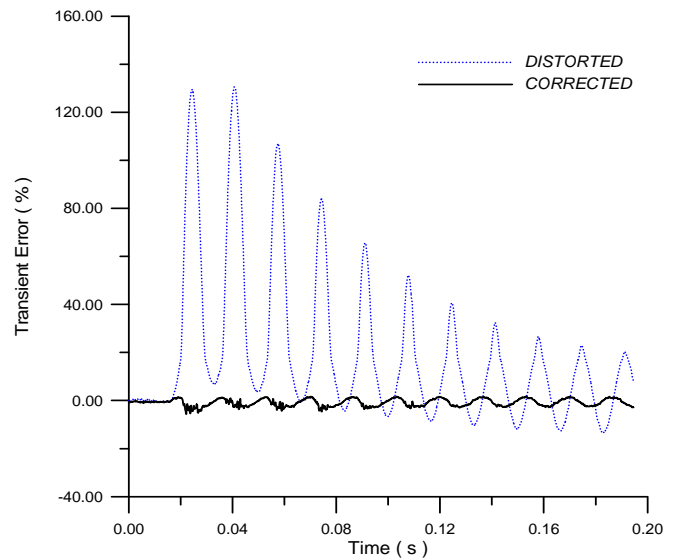


Fig. 18. Transient errors – Burden:  $1.0 + j 1.0 \Omega$ .

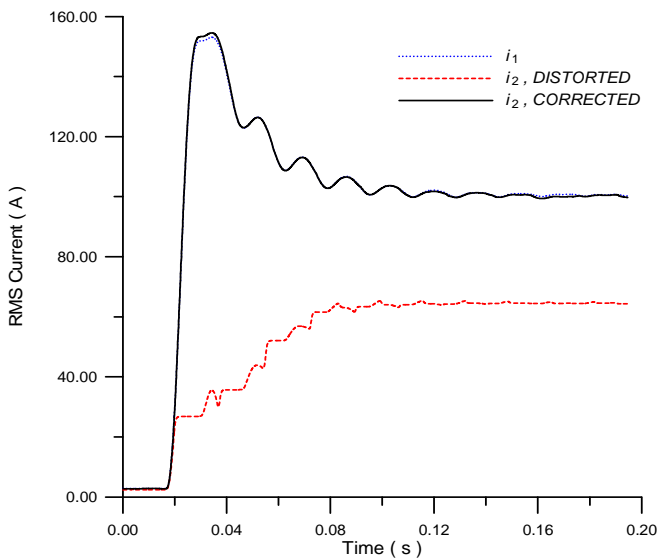


Fig. 16. RMS currents  $i_1$ ,  $i_2$  (distorted, corrected) – Burden:  $2.4 + j 0.7 \Omega$ .

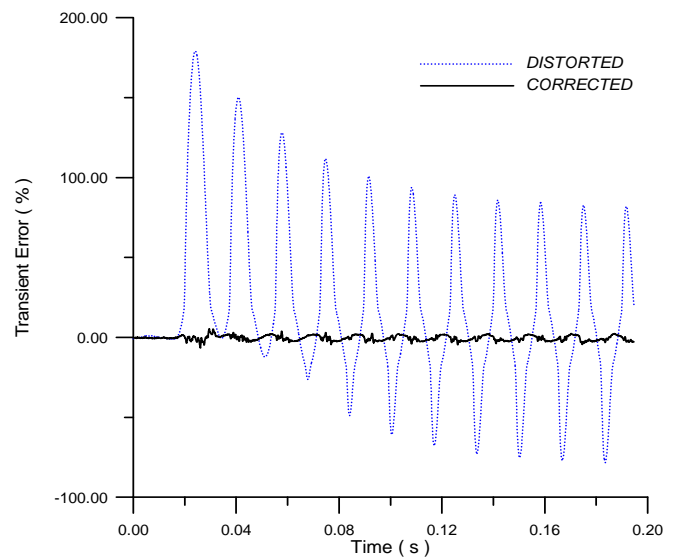


Fig. 19. Transient errors – Burden:  $2.4 + j 0.7 \Omega$ .

Table I shows the maximum transient errors,  $\varepsilon_T$ , that occur in the correction processes.

TABLE I  
MAXIMUM TRANSIENT ERRORS

Burden ( $\Omega$ )	$\varepsilon_T$ – distorted (%)	$\varepsilon_T$ – corrected (%)
$1.0 + j 0.0$	180.39	14.44
$1.0 + j 1.0$	130.48	-11.18
$2.4 + j 0.7$	179.19	-6.66

The presented results indicate that the proposed method corrects the distorted secondary current in a satisfactory way and that the errors introduced by the iron core CTs are significantly reduced.

## VII. CONCLUSIONS

The success of the secondary current correction is extremely dependent on the accurate determination of the initial flux in the instant of the fault occurrence. In other methods, the initial flux is determined by estimation. However, such processes can cause significant errors. In the proposed technique, the initial flux imposed by the primary current is measured by the integration of the tertiary voltage winding of the CT. Moreover, the gap reduces the residual flux to a negligible value.

The loss of accuracy caused by the increase of the exciting current is compensated by the numeric processing performed by the correcting system. So, it is possible to use the same type of CT in the protection and in the measurement schemes.

The proposed correction method avoids the CT oversizing. Thus, the magnetic core dimensions become smaller and the ratio and phase errors are reduced. The inserted air gap allows an additional reduction of the core, because the secondary time constant, the remanence and the magnetic induction decrease. Another advantage of this technique is that the knowledge of the impedances of the load, secondary winding and connection wires to calculate the secondary excitation voltage is not necessary. This practice causes significant errors, because such impedances are not always precisely known. Another problem is that any change of their values requests modifications in the settings of the algorithm.

The CT must have a tertiary winding. However, this is not a significant problem, because this type of CT is readily available in the trade. Many CTs are manufactured with two or more low current windings. Moreover, these characteristics can be specified in the proposal of acquisition of those devices, with practically no increase to the cost of the CT, because the current in tertiary winding is very low. In this case, the winding can be built with thin wire, which is only used for measurement of the induced voltage to calculate the magnetic flux in the iron core.

## VIII. ACKNOWLEDGMENT

The authors acknowledge the financial support provided by Chesf - Hydroelectric Company of São Francisco - Brazil, under Project No. 0048-035 ANEEL / 2010.

## IX. REFERENCES

- [1] F. C. F. Guerra and W. S. Mota, "Current Transformer Model," IEEE Trans. Power Del., vol. 22, no. 1, pp. 187-194, Jan. 2007.
- [2] D. A. Bradley, G. B. Gray, and D. O'Kelly, "Transient compensation of current transformers," IEEE Trans. Power App. Sys., vol. PAS-97, no. 4, pp. 1264-1271, 1978.
- [3] L. Masson, "Circuit for dynamic control of magnetic flux in current transformers," IEEE Trans. Power App. Sys., vol. PAS-98, no. 6, pp. 1990-1995, 1979.
- [4] T. Conrad and D. Oeding, "A method to correct the distorted secondary currents of current transformers," in Proc. PSCC, pp. 311-315, 1987.
- [5] Y. C. Kang, S. H. Kang, J. K. Park, A. T. Johns, and R. K. Aggarwal, "Development and hardware implementation of a compensating algorithm for secondary current of current transformers," IEE Proc. Power Appl., vol. 143, no. 1, pp. 41-49, Jan. 1996.
- [6] Y. C. Kang, S. H. Ok, S. H. Kang, and P. A. Crossley, "Design and evaluation of an algorithm for detecting current transformer saturation," IEE Proc. Gener. Transm. and Dist., vol. 151, no. 1, pp. 27-35, Jan. 2004.
- [7] Y. C. Kang, U. J. Lim, S. H. Kang, and P. A. Crossley, "Compensation of the distortion in the secondary current caused by saturation and remanence in a CT," IEEE Trans. Power Del., vol. 19, no. 4, pp. 1642-1649, Oct. 2004.
- [8] F. Li, Y. Li, and R. K. Aggarwal, "Combined wavelet transform and regression technique for secondary current compensation of current transformers," IEE Proc. Gener. Transm. and Dist., vol. 149, no. 4, pp. 497-50, Jul. 2002.
- [9] J. Pan, K. Vu, and Y. Hu, "An efficient compensation algorithm for current transformer saturation effects," IEEE Trans. Power Del., vol. 19, no. 4, pp. 1623-1628, Oct. 2004.
- [10] K. M. El-Naggar, and M. I. Gilany, "A discrete dynamic filter for detecting and compensating CT saturation," Elect. Power Syst. Research, vol. 77, pp. 527-533, 2006.
- [11] A. Hooshyar and M. Sanaye-Pasand, "Accurate measurement of fault currents contaminated with decaying DC offset and CT saturation" vol. 27, no. 2, pp. 773-783, Apr. 2012.
- [12] A. Wiszniewski, W. Rebizant, and L. Schiel, "Correction of current transformer transient performance," IEEE Trans. Power Del., vol. 23, no. 2, pp. 624-632, Apr. 2008.
- [13] D. C. Yu, J. C. Cummins, Z. Wang, H. J. Yoon, and L. A. Kojovic, "Correction of current transformer secondary currents due to saturation using artificial neural networks," IEEE Trans. Power Del., vol. 16, no. 2, pp. 189-194, Apr. 2001.
- [14] H. Khorashadi-Zadeh and M. S. Pasand, "Correction of saturated current transformers secondary current using ANNs," IEEE Trans. Power Del., vol. 21, no. 1, pp. 73-79, Jan. 2006.
- [15] E. C. Segatto and D. V. Coury, "Redes neurais artificiais recorrentes aplicadas na correção de sinais distorcidos pela saturação de transformadores de corrente," Revista Controle & Automação, vol. 17, no. 4, Out./Nov./Dec. 2006.